JCI insight

Steroid-sensitive nephrotic syndrome candidate gene CLVS1 regulates podocyte oxidative stress and endocytosis

Brandon M. Lane, … , Jameela A. Kari, Rasheed Gbadegesin

JCI Insight. 2021. https://doi.org/10.1172/jci.insight.152102.

Research In-Press Preview Nephrology

Graphical abstract

Title:

Steroid-sensitive nephrotic syndrome candidate gene CLVS1 regulates podocyte oxidative stress and endocytosis

Brandon M Lane[1], Megan Chryst-Stangl[1], Guanghong Wu[1], Mohamed Shalaby[2], Sherif El Desoky[2], Claire C Middleton[1], Kinsie Huggins[1], Amika Sood[3], Alejandro Ochoa[3], Andrew F Malone[4], Ricardo Vancini[5], Sara E Miller[5], Gentzon Hall[1,6], So Young Kim[7], David N Howell[5], Jameela A Kari[2], Rasheed Gbadegesin[1,6]

1. Department of Pediatrics, Division of Nephrology and Duke Molecular Physiology Institute, Duke University School of Medicine, Durham, NC 27710, USA
2. King Abdulaziz University, Pediatric Department, Pediatric Nephrology Center of Excellence, Jeddah, Kingdom of Saudi Arabia
3. Department of Biostatistics and Bioinformatics and Duke Center for Statistical Genetics and Genomics, Duke University, Durham, NC 27705, USA
4. Department of Medicine, Division of Nephrology, Washington University School of Medicine in St Louis, St. Louis, MO 63110, USA
5. Department of Pathology, Duke University School of Medicine, Durham, NC 27710, USA
6. Department of Medicine, Division of Nephrology, Duke University School of Medicine, Durham, NC 27710, USA
7. Department of Molecular Genetics and Microbiology, Duke University School of Medicine, Durham, NC 27710, USA

The authors have declared that no conflict of interest exists

Corresponding Author: Rasheed Gbadegesin, Carmichael building, 300 North Duke Street, Durham, NC 27701-2047, 919-684-4246, rasheed.gbadegesin@duke.edu,

Abstract:

We performed next generation sequencing in patients with familial steroid sensitive nephrotic syndrome (SSNS) and identified a homozygous segregating variant (p.H310Y) in the gene encoding clavesin-1 (*CLVS1*) in a consanguineous family with three affected individuals. Knockdown of the clavesin gene in zebrafish (clvs2) produced edema phenotypes due to disruption of podocyte structure and loss of glomerular filtration barrier integrity that can be rescued by WT *CLVS1* but not the p.H310Y variant. Analysis of cultured human podocytes with CRISPR-Cas9 mediated *CLVS1* knockout or homozygous H310Y knockin revealed deficits in clathrin-mediated endocytosis and increased susceptibility to apoptosis that could be rescued with corticosteroid treatment, mimicking the steroid-responsiveness observed in SSNS patients. The p.H310Y variant also disrupts binding of clavesin-1 to alpha-tocopherol transfer protein, resulting in increased reactive oxygen species (ROS) accumulation in *CLVS1*-deficient podocytes. Treatment of *CLVS1* knockout or homozygous H310Y knockin podocytes with pharmacological ROS inhibitors restored viability to control levels. Taken together, this data identifies *CLVS1* as a candidate gene for SSNS, provides insight into therapeutic effects of corticosteroids on podocyte cellular dynamics and adds to the growing evidence on the importance of endocytosis and oxidative stress regulation to podocyte function.

Introduction:

Childhood nephrotic syndrome (NS) is a common pediatric kidney disease estimated to affect 16/100,000 children worldwide.(1) In children, 80% of all cases of NS are steroid-responsive and are referred to as steroid sensitive nephrotic syndrome (SSNS). The mechanisms by which corticosteroids cause remission in NS and their effects on podocyte function and viability are not completely understood.

Nephrotic syndrome due to single-gene defects is found in 10-30% of patients depending on the population being studied.(2–4) Most cases of genetic NS are steroid resistant (SRNS) and are often due to defects in glomerular visceral epithelial cell (i.e. podocyte) structural proteins.(5,6) Podocytes are an essential cellular component of the kidney glomerular filtration barrier (GFB). SSNS, on the other hand, is largely considered an immune mediated disease; however, pathogenic variants in some genes involved in podocyte cytoskeletal dynamics have been reported in patients with SSNS.(6–10) Moreover, while corticosteroids can act as immunosuppressant, they can also have protective effects on podocytes through stabilization of the actin cytoskeleton. (11,12)

In this study, we identify a homozygous variant (c.928C>T, p.H310Y, ENST00000519846.1, rs139500383) in the gene encoding clavesin-1 (*CLVS1,* NC_000008.11) as a potential cause of SSNS in a consanguineous family with three affected individuals. CLVS1 is expressed in multiple human tissues including the kidney and brain, however studies to date have been limited to characterizations of its function in neurons.(13,14) Clavesin-1 is required for proper endosome formation and is suspected of having a role in clathrin-mediated endocytosis (CME) based on its ability to bind clathrin and phosphatidylinositol 3,5-bisphosphate.(13) Podocyte endocytosis is critical for the regulation of nephrin cycling and maintenance of the slit diaphragm with several endocytosis related genes having recently been established as contributors to podocyte dysfunction in NS.(15–21)

Our analysis reveals that the zebrafish clavesin gene is required for the maintenance of glomerular filtration barrier integrity *in vivo*. We confirmed the requirement for *CLVS1* in human podocyte homeostasis *in vitro* by demonstrating reduced viability and endocytosis in podocytes that are deficient in *CLVS1*, furthermore, we showed that this phenotype could be rescued with corticosteroid treatment. The p.H310Y variant is shown to be deleterious to clavesin-1 function *in vitro* and *in vivo* and affects binding to the ligand, alpha-tocopherol transfer protein. This reduced affinity for a transporter of the antioxidant alpha-tocopherol, causes an increased accumulation of reactive oxygen species (ROS) in *CLVS1* knockout and homozygous H310Y knockin podocytes. Moreover, pharmacological inhibition of ROS accumulation is sufficient to rescue the aberrant viability phenotype in podocytes with reduced functional clavesin-1, revealing new possible therapeutic strategies for patients with NS due to *CLVS1* defects and possible adjunct therapy for children with the more common idiopathic NS.

Results:

A rare variant in *CLVS1* is a likely cause of hereditary SSNS.

Next generation sequencing (whole genome or whole exome sequencing) was carried out in 42 sibling pairs with SSNS in our efforts to identify single-gene causes of SSNS. We subjected the sequencing data from each family to an established filtering algorithm for identification of single-gene causes of NS.(22) We identified a rare missense variant (c.928C>T, p.H310Y, NC_000008.11, rs139500383) in *CLVS1* as the only segregating variant candidate in Family DUK40585 (**Figure 1A**, **Supplementary Figure 1, and Supplementary Table 1**). We found homozygous variants in three other genes *(COL6A1, MX2, EML4)* that were present in affected individuals and unaffected siblings, but heterozygous in both parents (**Supplementary Table 1**). Family DUK40585 consists of unaffected consanguineous parents with 3 affected individuals comprising of two sisters and a paternal cousin (**Figure 1A**). All three affected individuals responded to corticosteroid treatment, although all three have frequent relapsing and steroid dependent course that was responsive to cyclophosphamide and rituximab (**Table 1**). Follow up data at eight and two years for individuals 1 and 100 showed that they are still in remission with normal kidney function **(Table 1).**

Homozygosity mapping of the affected family revealed that five significant region of homozygosity (ROHs) were present in both SSNS cases and absent in unaffected relatives (**Figure 1B** and **Supplementary Table 2**). The largest ROH located on chromosome 8 contains the *CLVS1* gene. None of the known single-gene causes of autosomal recessive nephrotic syndrome are located in these ROHs. (**Supplementary Table 2**).

The *CLVS1* gene exhibits a high degree of genetic constraint in humans with significantly fewer loss of function mutations reported in the general population than predicted, indicating that the product of this gene likely has important biological functions (pLI= 0.854).(23,24) The Histidine

residue at amino acid position 310 of clavesin-1 is highly conserved in evolution (**Table 2**) and the Tyrosine substitution found in the p.H310Y variant is predicted to be deleterious to clavesin-1 function by multiple *in silico* analyses (**Supplementary Table 1**). This variant is not present in a homozygous state in 281,974 chromosomes in the gnomAD database.(23) Sequencing of *CLVS1* in 604 additional patients with familial and sporadic NS of unclear etiology did not reveal other potentially pathogenic variants, suggesting that mutations in *CLVS1* are likely to be a very rare cause of familial SSNS.

Clavesin-1 is expressed in the podocyte

The expression and function of clavesin-1 in most tissues including the kidney has yet to be fully defined. We used immunofluorescence staining and immunoblotting to reveal the expression and co-localization of *CLVS1* with *WT1* proteins in podocytes from extracted mouse glomeruli (**Supplementary Figures 2A-B)**. While human podocyte *CLVS1* expression has already been reported in single-cell sequencing data collected from kidney tissue samples, we used immunoblotting to confirm the expression of *CLVS1* in conditionally immortalized human podocyte cell lines (**Supplementary Figure 2C-F)**.(25,26) Despite relatively high *CLVS1* expression in neuronal cells compared to podocytes, neurological abnormalities have not been reported in the family carrying the p.H310Y variant, suggesting that clavesin-1 may have podocyte cell-specific functions that are critical for maintenance of the GFB.

The zebrafish clavesin gene is required for maintenance of the GFB

As the p.H310Y variant is predicted to be damaging to clavesin-1 function, we examined the effects of reduced clavesin protein activity on glomerular function *in vivo* using morpholino mediated gene knockdown. The single zebrafish clavesin gene, *clvs2*, is the ortholog of human *CLVS2*, the paralog of *CLVS1*. While the H310 residue is not conserved, *clvs2* contains the major functional domains of both *CLVS1* and *CLVS2*, which allowed us to evaluate the requirement for

clavesin protein function in the maintenance of zebrafish GFB integrity. Knockdown of *clvs2* in zebrafish larvae using both translation blocking and splice blocking morpholinos was sufficient to induce edema phenotypes when compared to control morpholino injected fish at 4 days post fertilization (**Figures 2A-E**). We confirmed that the edema phenotypes in *clvs2* MO fish resulted from a disruption of the glomerular filtration barrier by quantifying the excretion of fluorescently labeled Vitamin D binding protein (a surrogate marker of albuminuria-sized protein leak) in the established Tg(lfabp::vdbp-GFP) reporter fish line (**Figure 2F**).(27) Podocyte foot process effacement was observed in *clvs2* MO larvae and not in control morphants (**Figure 2G-H**). The edema phenotype in *clvs2* MO larvae could be rescued by the addition of exogenous zebrafish *clvs2* mRNA as well as wild type human *CLVS1* mRNA but not by human *CLVS1* mRNA encoding the p.H310Y variant (**Figure 2E**). Taken together, this data suggests that there is an evolutionary requirement for clavesin proteins in the maintenance of glomerular filtration barrier integrity and that the p.H310Y variant disrupts clavesin-1 function.

Loss of *CLVS1* decreases human podocyte viability that can be rescued by corticosteroid treatment

To examine the requirement of functional clavesin-1 activity for the maintenance of human podocyte homeostasis, we created conditionally immortalized human podocyte cells lines with CRISPR-Cas9 mediated *CLVS1* knockout (KO). Additionally, to examine the specific effects of the H310Y variant, we used CRISPR-Cas9 gene editing to create heterozygous and homozygous *CLVS1* H310Y knockin (KI) podocyte lines. Automated live-cell imaging of caspase 3 enzymatic activity using a fluorescently labeled substrate of cleaved caspase 3 allowed for quantification of podocyte apoptosis over time (**Supplementary Videos 1-3**). Propidium iodide (PI) staining was used as a marker of late apoptosis and necrosis. When exposed to serum starvation over 72 hours, the *CLVS1* KO and homozygous H310Y KI displayed significantly increased apoptosis and total cell death compared to untransfected podocyte controls (**Figure 3** and **Supplementary**

Figure 3). Heterozygous H310Y KI podocytes displayed similar levels of apoptosis compared to controls, providing additional support for *CLVS1* in the development of autosomal recessive disease.

As the affected family with the *CLVS1* p.H310Y variant responded to corticosteroid treatment, we examined the effects of dexamethasone on *CLVS1* podocytes. We treated podocyte cell lines with 1uM dexamethasone during 72 hours of serum starvation. The addition of dexamethasone eliminated the increased apoptosis in *CLVS1* KO and homozygous KI podocytes compared to controls, mirroring the phenotype observed in the affected family (**Figure 3** and **Supplementary Figure 3**). These same corticosteroid-responsive apoptosis phenotypes were confirmed in podocyte cell lines with stable lentiviral shRNA-mediated *CLVS1* knockdown (KD) as well as HEK293 cells overexpressing the H310Y variant compared to their respective controls (**Supplementary Figures 4** and **5**).

CLVS1 is required for clathrin-mediated endocytosis in human podocytes

To understand the contributions of *CLVS1* deficits to reduced podocyte viability, we examined the impact on cellular endocytosis. Clavesin-1 has been shown to be required for proper endosome formation and its ability to bind both clathrin and phosphatidylinositol 3,5-bisphosphate suggests a role in clathrin-mediated endocytosis (CME).(13) We first examined podocyte endocytosis through the use of a 10,000 mW dextran compound (pHrodo) that is pH sensitive and fluoresces green when internalized within the cell. The number of internalized dextran molecules were quantified through the use of automated live cell imaging to compare the relative endocytosis between podocyte cell lines. *CLVS1* KO podocytes displayed decreased endocytosis of dextran when compared to their respective controls, demonstrating the importance of *CLVS1* function to endocytic processing in podocytes. (**Figure 4** and **Supplementary Figure 3**) Pre-treatment of *CLVS1* KO podocytes with dexamethasone restored the endocytosis of dextran to untreated podocyte control levels. These findings were again confirmed in *CLVS1* KD podocytes and

HEK293 cells overexpressing the H310Y variant compared to controls (**Supplementary Figures 4** and **5**).

Dextran molecules of this size are internalized through multiple modes of endocytosis including macropinocytosis, caveolae-mediated endocytosis, and CME. To identify the specific forms of endocytosis affected by deficiencies in *CLVS1*, we used automated cell imaging to quantify the internalization of fluorescently labeled transferrin and albumin molecules in cultured human podocytes. Transferrin molecules are internalized through CME while albumin molecules undergo caveolae-mediated endocytosis. As can be seen in **Figure 5**, *CLVS1* KO and H310Y homozygous KI podocytes displayed decreased clathrin-mediated endocytosis that was unresponsive to corticosteroid treatment. Caveolae-mediated endocytosis however, was unaffected by the loss of *CLVS1* or the H310Y variant. While macropinocytosis was also unaffected in *CLVS1* KO and H310Y cell lines, the treatment with steroids did provide a significant increase in macropinocytosis in all podocyte cell lines. This data confirms the suspected role for clavesin-1 in CME and suggests that CME-independent corticosteroid-responsive mechanisms including macropinocytosis likely contribute to the phenotype rescue in *CLVS1* KO and H310Y KI podocytes.

The *CLVS1* p.H310Y variant disrupts *CLVS1* ligand binding

Three-dimensional predictive modeling of the wild type clavesin-1 protein and the p.H310Y variant reveals that this mutation will likely produce a significant structural change to the c-terminus of the protein that will affect ligand binding (**Figure 6A**). While the c-terminus of clavesin-1 is important for clathrin binding and is likely to be severely impacted, the ligand predicted to be most affected by this structural alteration is the alpha-tocopherol transfer protein (αTTP) bound to alpha-tocopherol (**Supplementary Figure 6**). Alpha-tocopherol is the main functional component of Vitamin E present in humans, where it functions as an antioxidant due to its free radical scavenging abilities.(28–31) Treatment with alpha-tocopherol has been shown to have a protective

effect on podocytes in mouse models of glomerular disease.(32–37) We confirmed the p.H310Y mediated disruption of clavesin-1 binding to αTTP through co-immunoprecipitation studies in HEK293 cells transfected with Flag-tagged αTTP and either Myc-tagged WT or p.H310Y *CLVS1* constructs in the presence of excess alpha-tocopherol (**Figure 6B-C and Supplementary Figure 7**).

CLVS1 KO and H310Y KI podocytes generate increased reactive oxygen species

To determine if the altered intracellular trafficking of a key antioxidant like alpha-tocopherol can affect podocyte oxidative stress regulation, we examined the accumulation of reactive oxygen species (ROS) in *CLVS1* KO and H310Y KI podocytes. Using automated live cell imaging and fluorescent reporters of multiple ROS types, we quantified podocyte ROS generation with a reporter that detects hydrogen peroxide, peroxynitrite, and hydroxl radicals (**Figure 7A**) as well as a separate reporter for superoxide generation (**Figure 7B**). *CLVS1* KO and H310Y homozygous KI podocytes both displayed increased levels of ROS accumulation that could be restored to control podocyte levels with corticosteroid treatment.

Furthermore, to investigate the potential contribution of these increased ROS levels to deficits in *CLVS1* podocyte viability, we treated *CLVS1* KO podocytes with compounds targeting decreased ROS accumulation and examined their effects on apoptosis. Treatment with Elamipretide, an inhibitor of mitochondrial ROS generation, and MitoTEMPO, a mitochondrial targeted superoxide scavenger was sufficient to restore podocyte viability in *CLVS1* KO podocytes (**Figure 7C,D**). Taken together, this data suggests that oxidative stress regulation may be compromised in patients carrying the *CLVS1* p.H310Y variant and that increased ROS accumulation is likely a contributing factor in *CLVS1*-mediated NS. Moreover, drugs targeting ROS accumulation and oxidative stress represent possible therapeutic options for these patients.

Discussion:

In the present study, we showed that *CLVS1* encodes an essential component of podocyte CME and that a rare homozygous variant in this gene (p.H310Y) is a potential cause of corticosteroid-responsive NS. The p.H310Y variant was deleterious to clavesin-1 function, resulting in corticosteroid-responsive phenotypes in human podocytes including increased ROS accumulation and decreased viability. While the possible contributions of the other three variants found in this study cannot be completely discounted, the accumulated genetic and functional data in this study indicates that *CLVS1* is a candidate gene for autosomal recessive SSNS.

The loss of *CLVS1* resulted in defective podocyte endocytosis, suggesting that proper regulation of these vesicle pathways is critical to maintenance of the glomerular filtration barrier (GFB). This vital role for podocyte endocytosis in NS is supported by recent findings by other investigators. Both clathrin-dependent and clathrin-independent endocytosis serve critical roles in the regulation of podocyte associated slit diaphragm proteins including nephrin.(15–19) Mutations in endocytosis related proteins *GAPVD1, ANKFY1*, and *TBC1D8B* have now been identified as causes of monogenic NS.(20,21) Furthermore, disruption of key endocytosis related genes in murine models have been shown to be sufficient to induce proteinuria.(18,38,39) However, the molecular mechanisms responsible for disruptions in GFB integrity resulting from defective podocyte endocytosis have yet to be fully elucidated.

In addition to defects in podocyte endocytosis, *CLVS1* p.H310Y, is also predicted to disrupt the ligand binding site for αTTP bound to alpha-tocopherol. Alpha-tocopherol is a mitochondrial antioxidant that contributes to the regulation of lipid peroxidation and oxidative stress. The importance of mitochondrial antioxidants to glomerular disease has become an area of intense research as it has become increasingly apparent that increased oxidative stress is a common feature of chronic and progressive chronic kidney disease.(40–43) Mutations in genes related to coenzyme Q10, another mitochondrial associated antioxidant, including *PDSS1*, *PDSS2*, *COQ2*,

COQ6, and *COQ8B/ADCK4* are associated with the development of glomerular disease.(44–48) While mutations in αTTP are known to produce vitamin E deficiency associated with sensory ataxia in humans, its effects on kidney function are unclear.(49) However, the serum levels of vitamin E have been shown to fluctuate significantly between disease and remission states in patients with NS and are reported to be reduced in those with a frequent relapse disease course.(50–58) Moreover, vitamin E deficiency can lead to abnormal kidney development in murine models of disease.(59) Treatment with alpha-tocopherol has been reported to reduce proteinuria in multiple independent mouse models of glomerular and podocyte injury and has shown potential to improve proteinuria in NS patients as a supplemental treatment.(33,35–37,60,61) The discovery of a pathogenic mutation in SSNS patients that has the potential to alter vesicle trafficking of alpha-tocopherol in podocytes provides further evidence of the importance of podocyte ROS regulation and mitochondrial performance for maintaining the integrity of the GFB.

We have demonstrated that dexamethasone treatment can rescue the decreased podocyte endocytosis and viability phenotypes that result from the loss of *CLVS1* expression and the homozygous H310Y variant. It is currently unknown if this restored podocyte viability is a product of the corticosteroid induced increase in podocyte macropinocytosis to compensate for deficits in CME, or if there are additional cellular processes affected by dexamethasone treatment that contribute to the phenotype rescue. In addition to the potential endocytosis-related contributions to podocyte viability, dexamethasone may also directly affect podocyte ROS regulation, as glucocorticoids have been shown to increase antioxidant enzyme activities in rat models of glomerular disease.(62) While the mechanisms promoting this improved ROS processing have yet to be fully elucidated, our data demonstrates that increasing antioxidant activity and ROS scavenging can help restore the deficits in cell viability due to *CLVS1*.

Based on the analysis of *CLVS1* p.H310Y, we posit that this variant disrupts the CME of key podocyte molecules including alpha-tocopherol, leading to increased ROS accumulation and decreased podocyte viability (**Figure 8**). This reduction of podocyte health is at least partially restored by corticosteroid treatment due to an increase in macropinocytosis and ROS processing.

Limitations of our findings include the uncertainty of the contribution of the other three variants found in both affected and unaffected siblings to disease etiology and pathogenesis. In addition, it should be noted that the ancestry of the family in the present report (North African) is underrepresented in gnomAD, however, it is reassuring that we did not find any individual with the homozygous *CLVS1* H310Y variant in over 250,000 global exomes.

In conclusion, the discovery of another monogenic cause of SSNS that directly affects podocyte viability adds to the growing evidence which suggests that despite the major role of adaptive immunity in the pathogenesis of SSNS, primary or secondary disruption of podocyte cellular dynamics is a key component of NS pathogenesis regardless of the pattern of response to corticosteroids and other immunomodulatory treatment. Additionally, this data highlights the importance of endocytosis and ROS regulation to podocyte viability and provides insight into the therapeutic effects of corticosteroids on podocyte cellular dynamics. Continued evaluation of podocytes in the context of specific pathogenic variants like *CLVS1* p.H310Y will be critical to improving our understanding of disease pathogenesis and the development of new targeted therapies.

Methods:

Next Generation Sequencing: Next generation sequencing was performed at the Duke Center for Genomic & Computational Biology (GCB) and GENEWIZ (South Plainfield, NJ). Briefly, genomic DNA samples were assessed for purity, quantity, and quality by using the NanoDrop 2000 Spectrophotometer (Thermo Fisher), Qubit 2.0 Fluorometer and Qubit dsDNA HS Assay Kit

(Thermo Fisher), and agarose gel electrophoresis. Library construction was then performed using Illumina's TruSeq DNA PCR-free library preparation kit following the manufacturer's protocol. Genomic DNA was fragmented by acoustic shearing with a Covaris S220 instrument. Sheared DNA was then end-repaired and A-tailed, followed by adaptor ligation. Final libraries were analyzed on the Agilent TapeStation for library sizing, and quantified using the Qubit dsDNA HS Assay Kit and by qPCR using the KAPA Library Quantification Kit. DNA libraries were sequenced using Illumina platforms to generate ≥120Gb of raw data per sample with a 2x150bp paired-end sequencing configuration. Exome-Seq data was processed using the TrimGalore toolkit, which employs Cutadapt to trim low-quality bases and Illumina sequencing adapters from the 3' end of the reads.(63) Reads were aligned to the b37 version of the human genome with the BWA algorithm.(64) PCR duplicates were flagged using the PICARD Tools software suite. Alignment processing and variant calling were performed using the GATK toolkit following the Broad Institute's Best Practices Workflow.(65,66) Ensembl Variant Predictor (version 95) was used to annotate variant consequences and allele frequencies from gnomAD (exomes and genomes release 2.1) as well as the Exome Sequencing Project (ESP6500).(24,67,68) Once annotated, variants were filtered for quality using GATK's Variant Score Quality Recalibration workflow when able, otherwise the Broad's recommended 'hard-filtering' strategy was used. We retained variants at sites not in gnomAD or having an allele frequency less than 0.05 (in any population).

Variant Calling and Annotation: DNA-Seq data was processed using fastp1 to trim low-quality bases and Illumina sequencing adapters from the 3' end of reads.(69) Reads were then aligned to the GRCh37 version of the human genome with the BWA2 algorithm.(64) PCR duplicates were flagged using the PICARD Tools[3] software suite.(70) Alignment processing and variant calling were performed using the GATK4 toolkit following the Broad Institute's Best Practices Workflow.(65,66) Functional consequences and genotype provenances of variants were

annotated using Ensembl Variant Predictor.(67) Following annotation, variants meeting the following criteria were selected for further analysis: having a status of PASS following GATK's Variant Quality Score Recalibration; found to reside in a coding region; and had an allele frequency of less than 5 percent in at least one population of gnomAD.(23) Second level filtering to identify disease-causing variants is as shown in Supplementary Figure 1. Variants of interest were confirmed by Sanger sequencing.

Homozygosity Mapping: Kinship between individuals was estimated using the plink2 software applying the KING-robust estimator to the whole-exome data.(71,72) Runs of homozygosity (ROH) were estimated using the hidden Markov model implemented in the bcftools software module roh.(73) The human recombination map was used, and only variants with FILTER="PASS" and which were not indels were used in the analysis. Only ROH exceeding 1Mb in length were considered. ROH after filters (present in SSNS patients and absent in unaffected individuals) were merged if the gap between region pairs was less than 1Mb.

3D in silico protein modeling: For clavesin-1 modeling, I-TASSER generated a large ensemble of structural conformations, called decoys, based on the amino acid composition. To select the final models, I-TASSER uses the SPICKER program to cluster all the decoys based on the pair-wise structure similarity, and reports up to five models which corresponds to the five largest structure clusters. The confidence of each model is quantitatively measured using a C-score that is calculated based on the significance of threading template alignments and the convergence parameters of the structure assembly simulations.(74–76) For clavesin-1 ligand binding predictions, analysis was performed by COFACTOR and COACH based on the I-TASSER structure prediction. COFACTOR deduces protein functions using structure comparison and protein-protein networks, and COACH is a meta-server approach that combines multiple function annotation results (on ligand-binding sites) from the COFACTOR, TM-SITE and S-SITE programs.(77–80) Molecular graphics and analyses of PDB files created in the I-Tasser software

was performed with UCSF ChimeraX, developed by the Resource for Biocomputing, Visualization, and Informatics at the University of California, San Francisco, with support from National Institutes of Health R01-GM129325 and the Office of Cyber Infrastructure and Computational Biology, National Institute of Allergy and Infectious Diseases.

Zebrafish Analysis: All studies performed in zebrafish were approved by the Duke University Institutional Animal Care and Use Committee (IACUC). We designed a translation blocking (GGCCTGCCTGTAAATGAGTCATTGT) as well as a splice blocking MO (AAAATCCAATAGCTTCCTACCTGCT) targeting the exon1/intron1 splice site of clvs2 (Ensembl ID: ENSDART00000075112.6; Gene Tools). To determine MO efficiency, we injected 8 ng of each MO or a control MO (Gene Tools) into WT zebrafish embryos (ZDR) at the 1-4 cell stage (1 nl / embryo) and harvested them at 2 days post fertilization (dpf) for RNA extraction (splice blocking MO) and at 3 days for protein extraction (translation blocking MO). For analysis of splice blocking MO efficiency, we used the Qiashedder and RNAeasy mini kit (Qiagen) to extract RNA following the manufacturer's protocol and Promega Reverse Transcription kit to perform RT-PCR, and amplified the clvs2 targeted region using custom primers (F-CTCCTGGCCCAATACTTTGA and Rev-TCCGGGTCTTCTATCATTGC). To assess the efficiency of the translation blocking morpholino, we processed the embryos as described by O'Shea and Watterson. Briefly, 50 embryos were washed dechorionated with pronase before being the yolks were removed in Ringers solution containing PMSF and proteinase inhibitors. The remaining tissue was homogenized in 100µl of 2x SDS and boiled for 5 mins before performing immunoblotting as described below. We assessed the phenotypic effects of progressive doses of MO (3 ng, 5 ng and 8 ng) and subsequently used 5ng MO for the translation blocking morpholino and 8 ng for the splice blocking morpholino studies. For mRNA rescue, we obtained custom oligos with the WT zebrafish clvs2 ORF, WT human *CLVS1* ORF, and human *CLVS1* p.H310Y ORF (GenScript, Piscataway NJ). All constructs were created in a pcDNA3.1 backbone and were sequence

confirmed. To perform in vitro transcription, we linearized plasmids with NotI, and generated capped mRNA using the mMessage mMachine T7 Ultra transcription kit (ThermoFisher). We injected 150 pg mRNA for all embryo injections. Live bright field images were acquired on 4 dpf larvae anesthetized with tricaine using a Nikon AZ100 microscope with a Digital Sight color camera and NIS elements software.

Zebrafish GFB Evaluation: To examine the effects of clvs2 knockdown on the maintenance of GFB integrity, we took advantage of an established fish model for proteinuria detection (Tg(lfabp:VDBP-GFP)). This line contains a fluorescently labeled vitamin D molecule which is excreted when there are defects in GFB integrity. We injected clvs2 translation blocking morpholinos and control morpholinos as described above into 1-2 cell embryos resulting from breeding wild type fish to the GFP reporter line. Embryos were raised until 3 dpf and then transferred to a 24 well plate in groups of 3 with 500 µl of embryo water for 72 hours. Water was then collected and analyzed using a GFP ELISA kit (Boster Bio) according to the manufacturer's protocol.

Zebrafish Electron Microscopy: 5 dpf zebrafish embryos were fixed in 2.5% glutaraldehyde in 0.1M Sodium cacodylate buffer and washed the specimen in 0.1M sodium cacodylate buffer, 3 changes for 15 minutes each. Samples were post-fixed in 1.0% OsO_4 in 0.10 M sodium cacodylate buffer for 1 hour on the rotator and washed in 3 changes of working buffer, 15 minutes each change. Samples were then placed into *en bloc* stain (1% uranyl acetate) for 2h at RT and dehydrated in a series of ascending acetone concentration [50%, 75%,95%, 100% (X3)] for 10 minutes each. Specimens were placed in a 50/50 mixture of EPON/ACETONE overnight on a rotator before being replaced with 100% epoxy resin (EPON) for at least 2h at room temperature on a rotator. Then 2 more changes of 100% epoxy and incubated at least another 2h at room temperature on a rotator. Samples were then embedded in Beem capsules for 48h at 60°C and were ultrathin sectioned (60-70nm) on a Reichert Ultracut E ultramicrotome. Grids were stained

with 2% Uranyl acetate in 50% Ethanol for 30min and SATO's Lead stain for 1 min and imaged on a JEOL 2100plus electron microscope. Images were evaluated by a pathologist blinded to treatment groups.

Human podocyte cell lines: Conditionally immortalized human podocytes (courtesy of Dr. Jefferey Kopp) were grown, maintained, and differentiated as described previously.(81,82) To create the *CLVS1* knockdown lines, we used lentiviral particles containing shRNA against *CLVS1* (Sigma Aldrich). Lentiviral podocyte control lines were made using lentiviral particles containing non-targeted shRNA and knockdown was confirmed through Western Blot analysis.(76)

CRISPR Cas-9 mediated *CLVS1* knockout in the conditionally immortalized human podocytes was performed by the Duke Functional Genomics Core. Paired sgRNAs targeting exon 3 of *CLVS1* were designed using ChopChop (sgRNA 1- GGAAGTCCTAATCGAAGATC, sgRNA 2-ATGACAGCAGGATGGCACGA).(83) The sgRNAs were ordered as modified synthetic sgRNAs from Synthego. 1 x 10e5 podocytes were electroporated with 15 pmol sgRNA complexed with 15 pmol TrueCut Cas9 protein v2 (ThermoFisher Scientific) using a Neon system (ThermoFisher Scientific) with the following settings: 1300 V, 20 ms, 2 pulses. Cells were recovered on collagen coated 6 well plates for a period of a week, followed by plating at limiting dilution onto collagen-coated 96 well plates. Clones were expanded for several weeks and screened using PCR-sequencing to confirm out-of-frame insertions or deletions. Selected clones were also sequenced by TA cloning and Sanger sequencing to further confirm the presence of frameshifting indels (**Supplementary Figure 8)**. The lines were evaluated independently before being combined in the final analysis for clarity. Unmodified human podocytes were used as control comparisons for the CRIPSR KO lines.

Knockin (KI) podocytes created to introduce the c. 928T, p. H310Y mutation into the coding sequence of *CLVS1*. 1x10e5 podocytes were electroporated with 15 pmol sgRNA complexed with 15 pmol TrueCut Cas9 protein v2 (ThermoFisher Scientific) and 10 pmol of single stranded

oligonucleotide donor using a Neon system (ThermoFisher Scientific) with the following settings: 1300 V, 20 ms, 2 pulses. The sgRNA (GAAGCATACGTCCTCGAATC) was ordered as modified synthetic sgRNA from Synthego. The oligo donor sequence was designed with the desired mutation as well as two additional silent mutations to prevent recleavage by Cas9 after HDR. The donor sequence is shown below and was ordered as an Ultramer with two phosphorothioate bonds at each end from Integrated DNA Technologies. After electroporation, cells were recovered on collagen coated 6 well plates for a period of a week, followed by plating at limiting dilution onto collagen-coated 96 well plates. Clones were expanded for several weeks and screened by PCR using a primer pair that specifically detects the KI sequence. Positive clones were then subjected to PCR sequencing to confirm the presence of the desired genomic alterations (**Supplementary Figure 9).**

(donor:gcgatgaaaatgactatactcacacatcctataatgcaatgcacgtgaagtatacttcttcgaatctggagagagaatgctcacccaagctgatgaaaag)

HEK293 Cell Transfection: For the studies, human embryonic kidney cells (HEK293) cells were grown in Dulbecco's Modified Eagle medium (DMEM) supplemented with 10% fetal calf serum, penicillin (100U/ml), and streptomycin (100µg/ml) (all from Gibco, Gaithersburg, MD) as previously described.(84) For transfection, HEK293 cells were plated in 6 well tissue culture plates (Costar Corning, NY) and grown to ~80% confluency. Cells were then co-transfected with the Flag-tagged calcineurin TTPA construct (GenScript, Piscataway, NJ) and the Myc-tagged *CLVS1* construct (wild type or p.H310Y mutant as indicated) (GenScript) using Lipofectamine 2000 according to the manufacturer's recommendations (ThermoFisher Scientific, Waltham, MA).

Co-Immunoprecipitation studies: To achieve overexpression of tagged *TTPA* and *CLVS1* constructs, we used HEK293 cells due to the relative ease of transfection. Cells were harvested ~68 hours after transfection with Flag-tagged calcineurin TTPA and one of the Myc-tagged *CLVS1* constructs. Co-Immunoprecipitation was achieved using a Flag Immunoprecipitation kit (Sigma

Aldrich) and a Myc-tag Co-IP kit (ThermoFisher Scientific) according to the manufacturers' protocols. Immunoblotting was performed as described below for the immunoprecipitation lysates as well as input lysates to ensure equal loading between samples.

Automated Cell Apoptosis Imaging: To both visualize and quantify the apoptosis and total cell death in *CLVS1* KO podocytes and transfected HEK293 cells, we used a Lionheart FX automated microscope from BioTek along with fluorescent apoptosis reagents. Cells were grown in 96 well plates before exposure to serum free media containing a 1:500 dilution of NucView Caspase-3 Alexa488 (Biotium) and a 1:2000 dilution of Propidium Iodide (Sigma Aldrich). The NucView reagent consists of a substrate of Caspase-3 that emits green fluorescence when cleaved, while Propidium Iodide fluoresces in late apoptotic and necrotic cells. This media also contained either 1uM Dexamethasone or an equal concentration of vehicle (EtOH). Brightfield images along with green and red fluorescent images were collected every 2 hours for 48 hours. Using automated GEN5 software from BioTek, the images were processed to remove background and the number of fluorescent cells was quantified for each well using label free cell counting. Wells containing full serum were used as a control to test the validity of the apoptosis readings. The experiments were repeated in quadruplicate with a total N of at least 16 for each cell type.

Endocytosis assays: To measure general endocytosis in human podocyte cells and HEK293 cells, we used a 10,000 MW pHrodo green fluorescently labeled dextran (ThermoFisher). Cells were plated in 96 well pates. Podocyte plates were collagen coated. Cells were grown to 80% confluence and then washed twice with PBS and then exposed to a 1:75 dilution of pHrodo in imaging solution for 25 mins at 37 degrees Celsius, before it was removed and replaced with fresh imaging media and immediately imaged with the Lionheart FX automated microscope (BioTek). Fluorescently labeled molecules CF-Transferrin (Biotium), CF-Bovine Serum Albumin (Biotium), and Texas Red- Dextran 70,000 MW (ThermoFisher Scientific) were used to examine podocyte CME, caveolae-mediated endocytosis, and macropinocytosis respectively according the

manufacturer's protocols. Briefly cells were exposed to serum free media for 1 hr and before adding the transferrin, albumin, and dextran reagents (1mg/ml, 2mg/ml, 1mg/ml in PBS respectively). Podocytes were incubated at 37 degrees in the dark for 90 minutes and then washed twice with PBS followed by imaging media and imaged with the Lionheart FX. Using automated GEN5 software from BioTek, all images were processed to remove background and the number of fluorescent molecules per cell was quantified for each well using label free cell counting. For dexamethasone rescue, cells were exposed to 1μM Dexamethasone for 3 hrs before the beginning the assay.

Reactive Oxygen Species Quantification: To visualize and quantify the ROS accumulation within podocytes, we used the ROS-ID Total ROS Detection Kit (Enzo Biosciences) according to the manufacturer's protocol for the quantification of ROS including hydrogen peroxide, peroxynitrite and hydroxl radicals. Briefly podocytes cultured in collagen coated 96 well plates. Media was replaced with ROS detection solution and imaged every 20 mins over 1 hour using a Lionheart FX automated imaging system. Additionally, we used MitoSOX (ThermoFisher Scientific) for detection of mitochondrial superoxide. Briefly, we used 3.5μM of MitoSOX reagent in minimal media and imaged the cells every hour for 24 hours using the Lionheart FX imaging system. For dexamethasone rescue, cells were exposed to 1μM Dexamethasone for 3 hrs before the beginning the assays.

ROS inhibition: To examine the effects of reduced ROS levels on podocyte viability, we used 5nM Mito-TEMPO (Cayman Chemicals), 500nM of Elamipretide (MedChemExpress), and 10uM of alpha-tocopherol (Sigma Aldrich). All reagents were diluted 1:1000 from EtOH stock and added to serum free media alongside the apoptosis detection reagents.

Mouse glomerular immunofluorescence: We isolated mouse glomeruli from mouse kidneys by differential sieving with 180um, 100um, 71um metal sieves (Retsch) and washing with PBS (Gibco #10010-023). Glomeruli were plated onto a collagen I precoated flask (Corning #356484) and

cultured for 6 days with RPMI media (Gibco #11875-093) before an outgrowth of cobblestone-like cells were observed and harvested. Cells were fixed with 4% paraformaldehyde in PBS (Electron Microscopy Sciences t#15710) and washed with ice cold PBS three times before permeabilization with 0.1 Triton X-100 in PBS. Cells were then washed with wash buffer (0.5% BSA, 0.05% Triton X-100 in PBS) twice and blocked with buffer containing 5% goat serum, 1% BSA and 0.1% Triton X-100 in PBS before incubation with Rabbit polyclonal CLVS1 antibody (#PA5-32088 Invitrogen) and mouse monoclonal WT1 antibody (#sc-7385 Santa Cruz) overnight at 4'C. After additional washes, secondary Alexa Flora 488 and 568 antibodies were applied (Invitrogen) at a concentration of 1:400 for 1 hour at room temperature. Cells were then washed with wash buffer four times before addition of DAPI stain. Immunofluorescence imaging was performed using an EVOS FL imaging system.

Immunoblotting: Immunoblotting was performed using standard methods and visualized by enhanced chemiluminescence as previously described.(81) Antibodies were used at the following concentrations.CLVS1 (#C82727 Lifespan Biosciences and #PA5-32088 Invitrogen) 1:500, Beta-actin (#6609 Proteintech) 1:3000, Myc-tag (#PA1-981 Invitrogen) 1:800, DYKDDDDK (#D6W5B Cell Signaling Technologies) 1:800. Uncropped western blots are shown in **Supplementary Figure 10**.

Illustrations: The graphic abstract and Figure 8 were created with Biorender.com.

Statistics: Zebrafish larval batches were compared using $\chi 2$ tests (GraphPad software). One-way analysis of variance (ANOVA) followed by a Tukey HSD post hoc test was used to determine the differences between means for the analysis of endocytosis and immunoblotting results. Two-way ANOVA followed by a Dunnetts multiple comparisons analysis was used to compare groups over time for automated live cell apoptosis and ROS imaging. Statistical significance was established at $p<0.05$. All data are represented as the mean±SEM

Study Approval: All human studies were approved by the Duke University Medical Center Institutional Review Board and written informed consent was received from participants prior to inclusion in the study. Animal experiments were approved by the Duke University Medical Center Institutional Animal Care and Use Committees.

Author Contributions:

BL and RG designed the experiments and wrote the manuscript. All authors reviewed and edit the manuscript. Subject enrollment and sample acquisition was performed by MS, SE, JK, GH and RG. Sequencing and analysis of sequencing data was carried out by MCS, BL, and RG. BL, CM, and GW performed the experiments. Homozygosity mapping and analysis was performed by AS, AO, and KH. Single cell sequencing data analysis was performed by AM. CRISPR-Cas9 gene editing in podocytes was performed by SYK. RV and BL performed the electron microscopy while SM and DH evaluated the images for podocyte health.

Acknowledgements:

We acknowledge all the participants in the study. We appreciate the technical support provided by the Duke Molecular Physiology Institute (DMPI) genomics core and the personnel of Duke Center for Genomic & Computational Biology (GCB). RG is supported by National Institutes of Health/National Institutes of Diabetes and Digestive and Kidney Diseases (NIH/NIDDK) grants 5R01DK098135 and 5R01DK094987, NIH/NICHD 1R21HD104176-01, Doris Duke Charitable Foundation Clinical Scientist Development Award 2009033, Borden Scholars award, and Duke Health Scholars award. BL is supported by the Duke Nephrology T32 award (T32-DK007731). GH is supported by NIH/NIDDK grant 1K08DK111940-01.

References

1. Niaudet P. Genetic forms of nephrotic syndrome. Pediatr Nephrol Berl Ger. 2004 Dec;19(12):1313–8.

2. Sadowski CE, Lovric S, Ashraf S, Pabst WL, Gee HY, Kohl S, et al. A single-gene cause in 29.5% of cases of steroid-resistant nephrotic syndrome. J Am Soc Nephrol JASN. 2015 Jun;26(6):1279–89.

3. Varner JD, Chryst-Stangl M, Esezobor CI, Solarin A, Wu G, Lane B, et al. Genetic Testing for Steroid-Resistant-Nephrotic Syndrome in an Outbred Population. Front Pediatr. 2018;6:307.

4. Sampson MG, Gillies CE, Robertson CC, Crawford B, Vega-Warner V, Otto EA, et al. Using Population Genetics to Interrogate the Monogenic Nephrotic Syndrome Diagnosis in a Case Cohort. J Am Soc Nephrol JASN. 2016;27(7):1970–83.

5. Bensimhon AR, Williams AE, Gbadegesin RA. Treatment of steroid-resistant nephrotic syndrome in the genomic era. Pediatr Nephrol Berl Ger. 2019 Nov;34(11):2279–93.

6. Gee HY, Ashraf S, Wan X, Vega-Warner V, Esteve-Rudd J, Lovric S, et al. Mutations in EMP2 cause childhood-onset nephrotic syndrome. Am J Hum Genet. 2014 Jun 5;94(6):884–90.

7. Gee HY, Zhang F, Ashraf S, Kohl S, Sadowski CE, Vega-Warner V, et al. KANK deficiency leads to podocyte dysfunction and nephrotic syndrome. J Clin Invest. 2015 Jun;125(6):2375–84.

8. Roberts ISD, Gleadle JM. Familial Nephropathy and Multiple Exostoses With Exostosin-1 (EXT1) Gene Mutation. J Am Soc Nephrol. 2008 Mar 1;19(3):450–3.

9. Park E, Chang HJ, Shin JI, Lim BJ, Jeong HJ, Lee KB, et al. Familial IPEX syndrome: different glomerulopathy in two siblings. Pediatr Int Off J Jpn Pediatr Soc. 2015 Apr;57(2):e59-61.

10. Ashraf S, Kudo H, Rao J, Kikuchi A, Widmeier E, Lawson JA, et al. Mutations in six nephrosis genes delineate a pathogenic pathway amenable to treatment. Nat Commun. 2018 May 17;9(1):1960.

11. Xing C-Y, Saleem MA, Coward RJ, Ni L, Witherden IR, Mathieson PW. Direct effects of dexamethasone on human podocytes. Kidney Int. 2006 Sep 2;70(6):1038–45.

12. Schonenberger E, Ehrich JH, Haller H, Schiffer M. The podocyte as a direct target of immunosuppressive agents. Nephrol Dial Transplant. 2011 Jan 1;26(1):18–24.

13. Katoh Y, Ritter B, Gaffry T, Blondeau F, Höning S, McPherson PS. The clavesin family, neuron-specific lipid- and clathrin-binding Sec14 proteins regulating lysosomal morphology. J Biol Chem. 2009 Oct 2;284(40):27646–54.

14. Uhlén M, Fagerberg L, Hallström BM, Lindskog C, Oksvold P, Mardinoglu A, et al. Tissue-based map of the human proteome. Science [Internet]. 2015 Jan 23 [cited 2021 Feb 21];347(6220). Available from: https://science.sciencemag.org/content/347/6220/1260419

15. Qin X-S, Tsukaguchi H, Shono A, Yamamoto A, Kurihara H, Doi T. Phosphorylation of Nephrin Triggers Its Internalization by Raft-Mediated Endocytosis. J Am Soc Nephrol. 2009 Dec 1;20(12):2534–45.

16. Quack I, Woznowski M, Potthoff SA, Palmer R, Königshausen E, Sivritas S, et al. PKCα Mediates β-Arrestin2-dependent Nephrin Endocytosis in Hyperglycemia*. J Biol Chem. 2011 Apr 15;286(15):12959–70.

17. Waters AM, Wu MYJ, Huang Y-W, Liu GY, Holmyard D, Onay T, et al. Notch Promotes Dynamin-Dependent Endocytosis of Nephrin. J Am Soc Nephrol. 2012 Jan 1;23(1):27–35.

18. Soda K, Balkin DM, Ferguson SM, Paradise S, Milosevic I, Giovedi S, et al. Role of dynamin, synaptojanin, and endophilin in podocyte foot processes. J Clin Invest. 2012 Dec 3;122(12):4401–11.

19. Babayeva S, Rocque B, Aoudjit L, Zilber Y, Li J, Baldwin C, et al. Planar Cell Polarity Pathway Regulates Nephrin Endocytosis in Developing Podocytes. J Biol Chem. 2013 Aug 16;288(33):24035–48.

20. Hermle T, Schneider R, Schapiro D, Braun DA, van der Ven AT, Warejko JK, et al. GAPVD1 and ANKFY1 Mutations Implicate RAB5 Regulation in Nephrotic Syndrome. J Am Soc Nephrol JASN. 2018 Aug;29(8):2123–38.

21. Dorval G, Kuzmuk V, Gribouval O, Welsh GI, Bierzynska A, Schmitt A, et al. TBC1D8B Loss-of-Function Mutations Lead to X-Linked Nephrotic Syndrome via Defective Trafficking Pathways. Am J Hum Genet. 2019 Feb 7;104(2):348–55.

22. Lane BM, Murray S, Benson K, Bierzynska A, Chryst-Stangl M, Wang L, et al. A Rare Autosomal Dominant Variant in Regulator of Calcineurin Type 1 (RCAN1) Gene Confers Enhanced Calcineurin Activity and May Cause FSGS. J Am Soc Nephrol JASN. 2021 Apr 16;

23. Karczewski KJ, Francioli LC, Tiao G, Cummings BB, Alföldi J, Wang Q, et al. The mutational constraint spectrum quantified from variation in 141,456 humans. bioRxiv. 2020 Apr 8;531210.

24. Lek M, Karczewski KJ, Minikel EV, Samocha KE, Banks E, Fennell T, et al. Analysis of protein-coding genetic variation in 60,706 humans. Nature. 2016 Aug;536(7616):285–91.

25. Wu H, Uchimura K, Donnelly EL, Kirita Y, Morris SA, Humphreys BD. Comparative Analysis and Refinement of Human PSC-Derived Kidney Organoid Differentiation with Single-Cell Transcriptomics. Cell Stem Cell. 2018 Dec 6;23(6):869-881.e8.

26. Wilson PC, Wu H, Kirita Y, Uchimura K, Ledru N, Rennke HG, et al. The single-cell transcriptomic landscape of early human diabetic nephropathy. Proc Natl Acad Sci. 2019 Sep 24;116(39):19619–25.

27. Zhou W, Hildebrandt F. Inducible podocyte injury and proteinuria in transgenic zebrafish. J Am Soc Nephrol JASN. 2012 Jun;23(6):1039–47.

28. Tappel AL. Vitamin E as the Biological Lipid Antioxidant. In: Harris RS, Wool IG, Marrian GF, Thimann KV, editors. Vitamins & Hormones [Internet]. Academic Press; 1962 [cited 2021 Feb 18]. p. 493–510. Available from: https://www.sciencedirect.com/science/article/pii/S0083672908607323

29. Burton GW, Ingold KU. Vitamin E: application of the principles of physical organic chemistry to the exploration of its structure and function. Acc Chem Res. 1986 Jun 1;19(7):194–201.

30. Esterbauer H, Dieber-Rotheneder M, Striegl G, Waeg G. Role of vitamin E in preventing the oxidation of low-density lipoprotein. Am J Clin Nutr. 1991 Jan;53(1 Suppl):314S-321S.

31. Chow CK, Ibrahim W, Wei Z, Chan AC. Vitamin E regulates mitochondrial hydrogen peroxide generation. Free Radic Biol Med. 1999 Sep;27(5–6):580–7.

32. Ricardo SD, Bertram JF, Ryan GB. Antioxidants protect podocyte foot processes in puromycin aminonucleoside-treated rats. J Am Soc Nephrol JASN. 1994 Jun;4(12):1974–86.

33. Washio M, Nanishi F, Okuda S, Onoyama K, Fujishima M. Alpha Tocopherol Improves Focal Glomerulosclerosis in Rats with Adriamycin-Induced Progressive Renal Failure. Nephron. 1994;68(3):347–52.

34. Hayashi D, Yagi K, Song C, Ueda S, Yamanoue M, Topham M, et al. Diacylglycerol Kinase alpha is Involved in the Vitamin E-Induced Amelioration of Diabetic Nephropathy in Mice. Sci Rep [Internet]. 2017 Jun 1 [cited 2021 Feb 18];7. Available from: https://www.ncbi.nlm.nih.gov/pmc/articles/PMC5453949/

35. Hayashi D, Ueda S, Yamanoue M, Ashida H, Shirai Y. Amelioration of diabetic nephropathy by oral administration of d-α-tocopherol and its mechanisms. Biosci Biotechnol Biochem. 2018 Jan;82(1):65–73.

36. Trachtman H, Chan JC, Chan W, Valderrama E, Brandt R, Wakely P, et al. Vitamin E ameliorates renal injury in an experimental model of immunoglobulin A nephropathy. Pediatr Res. 1996 Oct;40(4):620–6.

37. Stojiljkovic N, Ilic S, Veljkovic M, Todorovic J, Mladenovic M. α-Tocopherol Reduces Morphological Changes and Oxidative Stress during Gentamicin-Induced Acute Renal Failure. Bull Exp Biol Med. 2018 Mar;164(4):442–5.

38. Harris DP, Vogel P, Wims M, Moberg K, Humphries J, Jhaver KG, et al. Requirement for Class II Phosphoinositide 3-Kinase C2α in Maintenance of Glomerular Structure and Function. Mol Cell Biol. 2011 Jan 1;31(1):63–80.

39. Bechtel W, Helmstädter M, Balica J, Hartleben B, Kiefer B, Hrnjic F, et al. Vps34 Deficiency Reveals the Importance of Endocytosis for Podocyte Homeostasis. J Am Soc Nephrol. 2013 May 1;24(5):727–43.

40. Locatelli F, Canaud B, Eckardt K-U, Stenvinkel P, Wanner C, Zoccali C. Oxidative stress in end-stage renal disease: an emerging threat to patient outcome. Nephrol Dial Transplant Off Publ Eur Dial Transpl Assoc - Eur Ren Assoc. 2003 Jul;18(7):1272–80.

41. Hasselwander O, Young IS. Oxidative stress in chronic renal failure. Free Radic Res. 1998 Jul;29(1):1–11.

42. Annuk M, Zilmer M, Lind L, Linde T, Fellström B. Oxidative stress and endothelial function in chronic renal failure. J Am Soc Nephrol JASN. 2001 Dec;12(12):2747–52.

43. Dounousi E, Papavasiliou E, Makedou A, Ioannou K, Katopodis KP, Tselepis A, et al. Oxidative stress is progressively enhanced with advancing stages of CKD. Am J Kidney Dis Off J Natl Kidney Found. 2006 Nov;48(5):752–60.

44. Vasta V, Merritt JL, Saneto RP, Hahn SH. Next-generation sequencing for mitochondrial diseases: a wide diagnostic spectrum. Pediatr Int Off J Jpn Pediatr Soc. 2012 Oct;54(5):585–601.

45. López LC, Schuelke M, Quinzii CM, Kanki T, Rodenburg RJT, Naini A, et al. Leigh Syndrome with Nephropathy and CoQ10 Deficiency Due to decaprenyl diphosphate synthase subunit 2 (PDSS2) Mutations. Am J Hum Genet. 2006 Dec;79(6):1125–9.

46. Quinzii C, Naini A, Salviati L, Trevisson E, Navas P, DiMauro S, et al. A Mutation in Para-Hydroxybenzoate-Polyprenyl Transferase (COQ2) Causes Primary Coenzyme Q10 Deficiency. Am J Hum Genet. 2006 Feb;78(2):345–9.

47. Heeringa SF, Chernin G, Chaki M, Zhou W, Sloan AJ, Ji Z, et al. COQ6 mutations in human patients produce nephrotic syndrome with sensorineural deafness. J Clin Invest. 2011 May 2;121(5):2013–24.

48. Ashraf S, Gee HY, Woerner S, Xie LX, Vega-Warner V, Lovric S, et al. ADCK4 mutations promote steroid-resistant nephrotic syndrome through CoQ10 biosynthesis disruption. J Clin Invest. 2013 Dec 2;123(12):5179–89.

49. Ouahchi K, Arita M, Kayden H, Hentati F, Ben Hamida M, Sokol R, et al. Ataxia with isolated vitamin E deficiency is caused by mutations in the alpha-tocopherol transfer protein. Nat Genet. 1995 Feb;9(2):141–5.

50. Kinra S, Rath B, Kabi BC. Indirect quantification of lipid peroxidation in steroid responsive nephrotic syndrome. Arch Dis Child. 2000 Jan 1;82(1):76–8.

51. Mathew JL, Kabi BC, Rath B. Anti-oxidant vitamins and steroid responsive nephrotic syndrome in Indian children. J Paediatr Child Health. 2002 Oct;38(5):450–437.

52. Rajbala A, Sane AS, Zope J, Mishra VV, Trivedi HL. Oxidative stress status in children with nephrotic syndrome. Panminerva Med. 1997 Sep;39(3):165–8.

53. Ece A, Atamer Y, Gürkan F, Bilici M, Koçyiğit Y. Anti-oxidant status in relation to lipoproteins, leptin and pro-inflammatory cytokines in children with steroid-sensitive nephrotic syndrome. Nephrology. 2004;9(6):366–73.

54. Bafna DrA. Oxidant stress in primary nephrotic syndrome in relation to dyslipidemia. 2010 Jan 1;

55. El-Melegy NT, Mohamed NA, Sayed MM. Oxidative Modification of Low-Density Lipoprotein in Relation to Dyslipidemia and Oxidant Status in Children With Steroid Sensitive Nephrotic Syndrome. Pediatr Res. 2008 Apr;63(4):404–9.

56. Ghodake SR, Suryakar AN, Ankush RD, Katkam RV, Shaikh K, Katta AV. Role of free radicals and antioxidant status in childhood nephrotic syndrome. Indian J Nephrol. 2011;21(1):37–40.

57. Dwivedi J, Sarkar PD. International Journal of Pharma and Bio Sciences. (4):11.

58. Ghodake SR, Suryakar AN, Ankush RD, Shaikh K, Katta AV. Role of reactive oxygen species in pathogenesis of nephrotic syndrome. Indian J Clin Biochem IJCB. 2010 Jan;25(1):82–5.

59. Emmel VM. Studies on the Kidney in Vitamin E Deficiency: I. Post-Mortem Autolysis in Kidneys of Rats Fed a Vitamin E-Deficient Diet Rich in Long-Chain Unsaturated Fatty Acids. J Nutr. 1957 Jan 1;61(1):51–69.

60. Tahzib MN, Gauthier BG, Frank R, Trachtman H. Vitamin E Reduces Proteinuria in Children with Renal Disease • 1841. Pediatr Res. 1998 Apr;43(4):314–314.

61. Khatami PG, Soleimani A, Sharifi N, Aghadavod E, Asemi Z. The effects of high-dose vitamin E supplementation on biomarkers of kidney injury, inflammation, and oxidative stress in patients with diabetic nephropathy: A randomized, double-blind, placebo-controlled trial. J Clin Lipidol. 2016 Aug;10(4):922–9.

62. Kawamura T, Yoshioka T, Bills T, Fogo A, Ichikawa I. Glucocorticoid activates glomerular antioxidant enzymes and protects glomeruli from oxidant injuries. Kidney Int. 1991 Aug;40(2):291–301.

63. Martin M. Cutadapt removes adapter sequences from high-throughput sequencing reads. EMBnet.journal. 2011 May 2;17(1):10–2.

64. Li H, Durbin R. Fast and accurate short read alignment with Burrows-Wheeler transform. Bioinforma Oxf Engl. 2009 Jul 15;25(14):1754–60.

65. DePristo MA, Banks E, Poplin R, Garimella KV, Maguire JR, Hartl C, et al. A framework for variation discovery and genotyping using next-generation DNA sequencing data. Nat Genet. 2011 May;43(5):491–8.

66. Van der Auwera GA, Carneiro MO, Hartl C, Poplin R, Del Angel G, Levy-Moonshine A, et al. From FastQ data to high confidence variant calls: the Genome Analysis Toolkit best practices pipeline. Curr Protoc Bioinforma. 2013;43:11.10.1-11.10.33.

67. McLaren W, Gil L, Hunt SE, Riat HS, Ritchie GRS, Thormann A, et al. The Ensembl Variant Effect Predictor. Genome Biol. 2016 Dec;17(1):122.

68. Tennessen JA, Bigham AW, O'Connor TD, Fu W, Kenny EE, Gravel S, et al. Evolution and functional impact of rare coding variation from deep sequencing of human exomes. Science. 2012 Jul 6;337(6090):64–9.

69. Chen S, Zhou Y, Chen Y, Gu J. fastp: an ultra-fast all-in-one FASTQ preprocessor. Bioinformatics. 2018 Sep 1;34(17):i884–90.

70. Picard software [Internet]. Available from: http://broadinstitute.github.io/picard/

71. Chang CC, Chow CC, Tellier LC, Vattikuti S, Purcell SM, Lee JJ. Second-generation PLINK: rising to the challenge of larger and richer datasets. GigaScience. 2015;4:7.

72. Manichaikul A, Mychaleckyj JC, Rich SS, Daly K, Sale M, Chen W-M. Robust relationship inference in genome-wide association studies. Bioinformatics. 2010 Nov 15;26(22):2867–73.

73. Narasimhan V, Danecek P, Scally A, Xue Y, Tyler-Smith C, Durbin R. BCFtools/RoH: a hidden Markov model approach for detecting autozygosity from next-generation sequencing data. Bioinforma Oxf Engl. 2016 Jun 1;32(11):1749–51.

74. Yang J, Zhang Y. Protein Structure and Function Prediction Using I-TASSER. Curr Protoc Bioinforma. 2015 Dec 17;52:5.8.1-5.8.15.

75. Yang J, Zhang Y. I-TASSER server: new development for protein structure and function predictions. Nucleic Acids Res. 2015 Jul 1;43(Web Server issue):W174–81.

76. Roy A, Kucukural A, Zhang Y. I-TASSER: a unified platform for automated protein structure and function prediction. Nat Protoc. 2010 Apr;5(4):725–38.

77. Zhang C, Freddolino PL, Zhang Y. COFACTOR: improved protein function prediction by combining structure, sequence and protein-protein interaction information. Nucleic Acids Res. 2017 Jul 3;45(W1):W291–9.

78. Roy A, Yang J, Zhang Y. COFACTOR: an accurate comparative algorithm for structure-based protein function annotation. Nucleic Acids Res. 2012 Jul;40(Web Server issue):W471–7.

79. Yang J, Roy A, Zhang Y. Protein-ligand binding site recognition using complementary binding-specific substructure comparison and sequence profile alignment. Bioinforma Oxf Engl. 2013 Oct 15;29(20):2588–95.

80. Yang J, Roy A, Zhang Y. BioLiP: a semi-manually curated database for biologically relevant ligand-protein interactions. Nucleic Acids Res. 2013 Jan;41(Database issue):D1096-1103.

81. Hall G, Lane BM, Khan K, Pediaditakis I, Xiao J, Wu G, et al. The Human FSGS-Causing ANLN R431C Mutation Induces Dysregulated PI3K/AKT/mTOR/Rac1 Signaling in Podocytes. J Am Soc Nephrol JASN. 2018 Aug;29(8):2110–22.

82. Sakairi T, Abe Y, Kajiyama H, Bartlett LD, Howard LV, Jat PS, et al. Conditionally immortalized human podocyte cell lines established from urine. Am J Physiol - Ren Physiol. 2010 Mar;298(3):F557–67.

83. Labun K, Montague TG, Gagnon JA, Thyme SB, Valen E. CHOPCHOP v2: a web tool for the next generation of CRISPR genome engineering. Nucleic Acids Res. 2016 Jul 8;44(W1):W272-276.

84. Spurney RF. Role of C-terminal serines in desensitization and phosphorylation of the mouse thromboxane receptor. J Biol Chem. 1998 Oct 23;273(43):28496–503.

Figure 1: *CLVS1* p.H310Y is a potential cause of familial childhood SSNS A) Pedigree of family with SSNS showing segregation of the homozygous *CLVS1* p.H310Y variant (c.928C>T, GRCH37/hg19) with disease. Filled circle and square represent affected individuals, unfilled circle, square and diamond represent unaffected individuals. The parents of the family were estimated from their sequencing data to be 2nd-degree relatives (kinship coefficient of 0.106). **B)** Runs of homozygosity (ROH) potentially implicated in SSNS. The five ROHs (blue boxes, spanning each ROH on its respective chromosome) are those shared by both children with SSNS (ID 1 and 100), and are not in ROHs in any of the unaffected relatives that were sequenced (ID 1000, 1001, 101). Gene locations are marked with labeled red vertical lines. Candidate genes *CLVS1* and MX2 are located in these ROH regions.

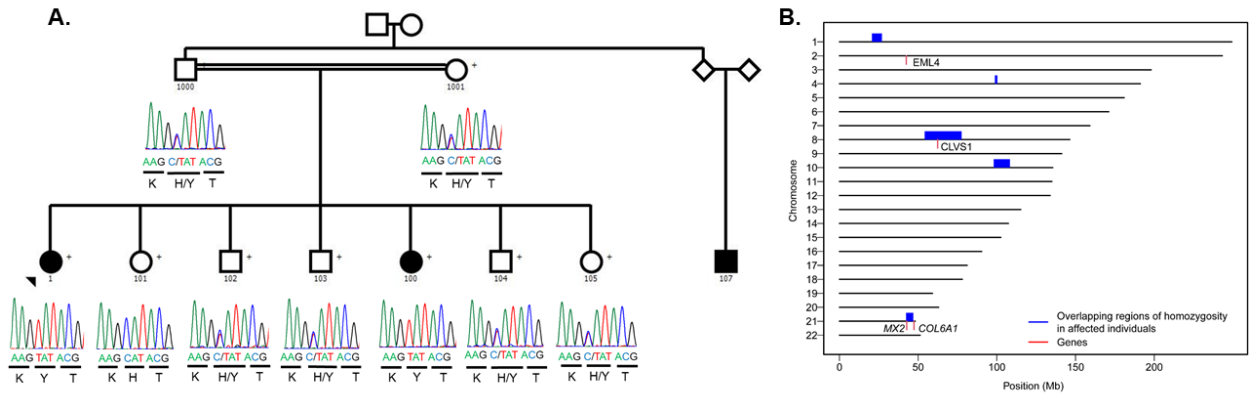

Figure 2: **Knockdown of the clavesin gene in zebrafish (*clvs2*) results in edema phenotypes. A-B)** Translation blocking and splice block morpholinos were used to knockdown clvs2 expression in zebrafish. Morpholino efficacy was confirmed through Western blot (A) and RT-PCR (B) show that both morpholinos were able to knockdown *clvs2* expression. **C)** Larval phenotypes were evaluated at 4 dpf as having edema (arrows for periorbital and pericardial) or unaffected (no edema). **D-E)** Analysis revealed significantly increased edema phenotypes with *clvs2* knockdown compared to controls and this edema could be rescued by co-injection of wild type human *CLVS1* mRNA but not the p.H310Y variant (E) (*=p<0.05, N>60 for all groups, one-way ANOVA). **F)** Quantification of excreted GFP-labeled Vitamin D in the Tg(lfabp:VDBP-GFP) reporter line revealed a loss of GFP in clvs2 morpholino injected fish compared to controls (n=10 for each group, p<0.0001, t-test), demonstrating that GFB integrity was affected by clvs2 knockdown. **G-H)** Transmission electron microscopy images show healthy podocyte foot processes with intact slit diaphragms (white arrowheads) around a capillary loop in 5 dpf control morphant larvae and podocyte effacement (red arrowhead) in *clvs2* morphants (scale bars = 800 nm and 1 µm respectively), confirming that edema phenotypes are due to reduced GFB integrity.

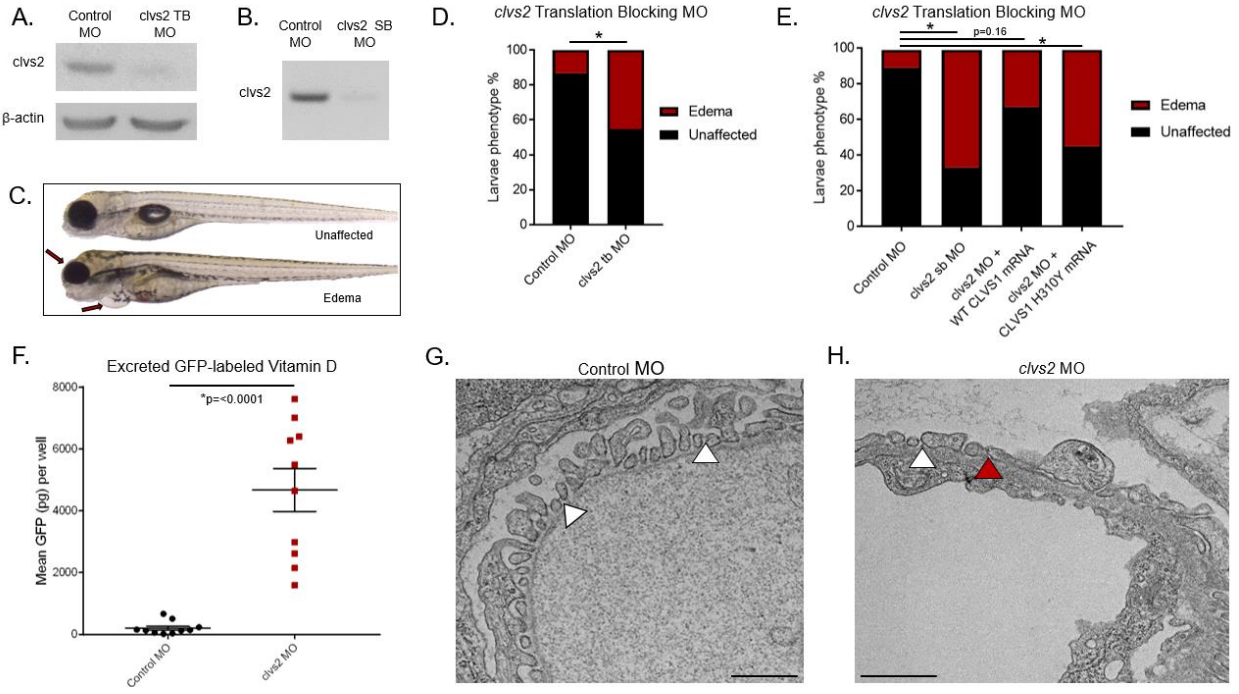

Figure 3: Loss of *CLVS1* expression increases podocyte susceptibility to apoptosis that can be restored by corticosteroid treatment. **A-B)** Western blot showing significantly reduced expression of *CLVS1* in CRISPR-Cas9 knockout (KO) podocyte cell lines compared with control cell lines (n=4, p<0.001, two tailed t-test). **C)** Still images depicting cleaved caspase 3 activity (green) as reporter for early apoptosis and propidium iodide staining (red) for late apoptosis and necrosis in human podocytes 72 hours post serum starvation (scale bars =1mm). **D)** Quantification of these images over time revealed an increase in podocyte susceptibility to serum starvation induced apoptosis in *CLVS1* KO and homozygous H310Y knockin (KI) podocytes compared to controls, (p<0.05 for all time points after 16 hours for KO and after 34 hours for KI, N>25 for each group, two-way ANOVA). Heterozygous H310Y KI podocytes displayed similar apoptotic phenotypes to controls. The elevated apoptosis in *CLVS1* KO and homozygous H310Y KI podocytes was rescued by treatment with 1µM Dexamethasone.

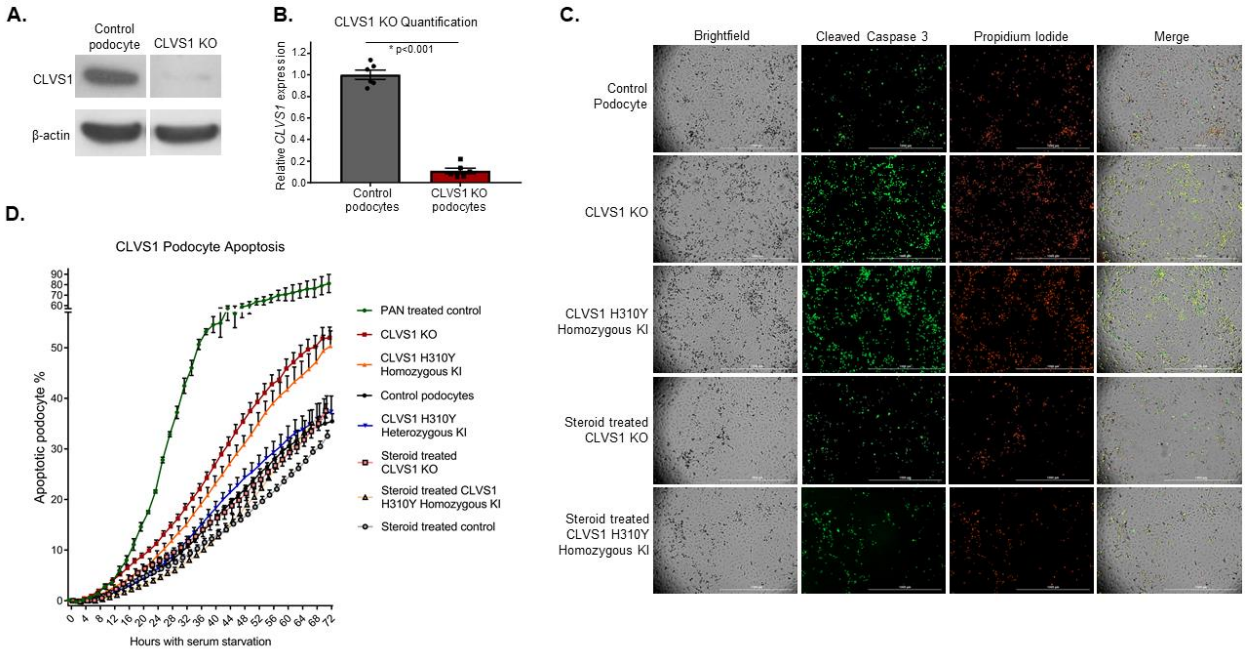

Figure 4: Loss of *CLVS1* causes decreased podocyte endocytosis. **A-C)** Images showing the decreased endocytosis of fluorescently labeled dextran (pHrodo Dextran) in conditionally immortalized podocytes with CRISPR-Cas9 mediated knockout of *CLVS1* that can be restored with treatment with 1µM dexmethasone (representative molecules circled in red). **D**) Quantification of these images revealed a significant (p=0.0193) loss of dextran endocytosis in KO podocytes compared to controls that was eliminated when these podocytes were treated with dexamethasone (p=0.7568, N>20 for each experimental group, one-way ANOVA). A selective inhibitor of dynamin I and dynamin II, Dynasore, which reduces clathrin-mediated endocytosis was used as an endocytosis control. Errors bars depict SEM

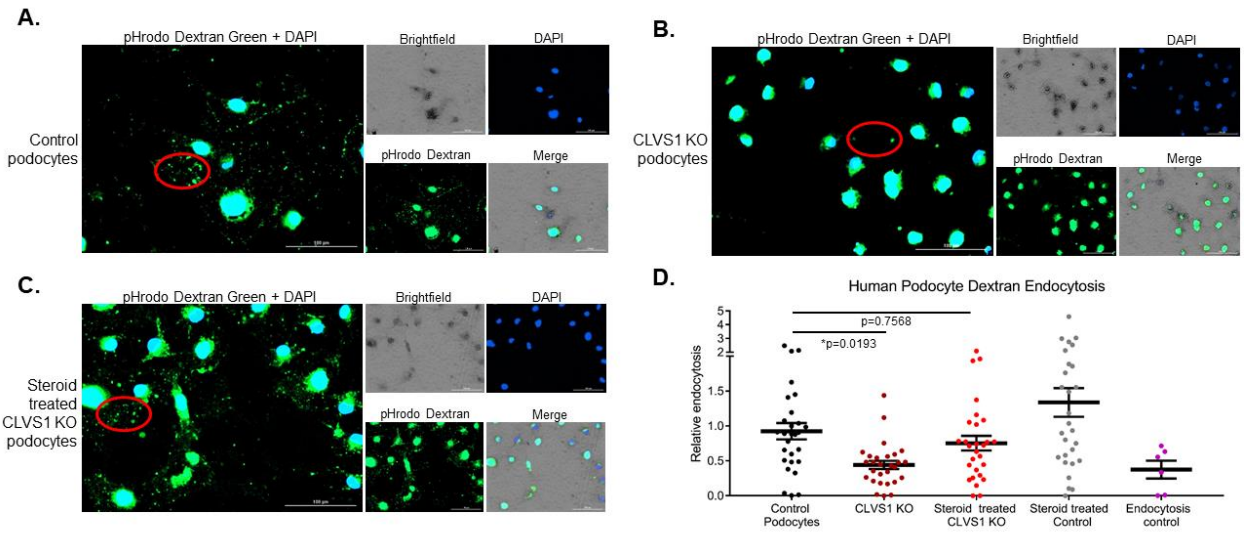

Figure 5: *CLVS1* is required for clathrin-mediated endocytosis in human podocytes. To examine specific modes of endocytosis in *CLVS1* podocytes, we evaluated the internalization of fluorescently labeled transferrin (clathrin-mediated endocytosis), 70,000 MW dextran (macropinocytosis), and albumin molecules (caveolae-mediated endocytosis). **A-B)** Quantification of the number of internalized transferrin molecules per cell revealed a decrease in clathrin-mediated endocytosis in *CLVS1* KO and homozygous H310Y KI podocytes compared to controls that was unaffected by pretreatment with 1uM dexamethasone. (N>30 for each group, p< 0.0001, one-way ANOVA) **C-D)** Macropinocytosis, as measured by the internalization of fluorescently labeled 70,000 MW dextran molecules, was unaffected by *CLVS1* KO or H310Y KI (p=0.9572 and p=0.9604 respectively, one-way ANOVA). However, treatment with dexamethasone did significantly increase macropinocytosis in all cell lines compared to vehicle treated controls (p<0.001 for all). **E-F)** Caveolae-mediated endocytosis was comparable between *CLVS1* KO, homozygous H310Y KI podocytes, and controls when internalized albumin molecules were quantified and this was unaffected by treatment with dexamethasone (N>30 for each group, p=0.993 and p=0.1844 respectively, one-way ANOVA). Error bars depict SEM in graphs. Scale bars = 12 µM. Each dot in the graphs represents the mean number of molecules per podocyte for a single well.

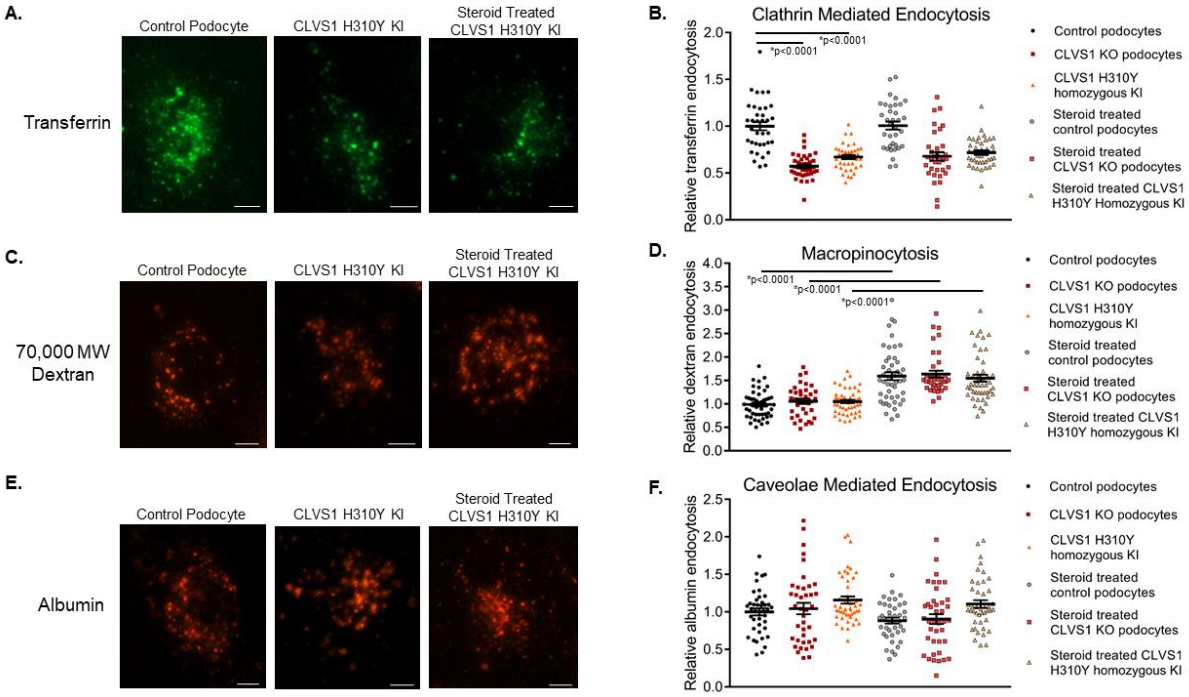

Figure 6: The *CLVS1* p.H310Y variant decreases clavesin-1 ligand binding to alpha-tocopherol transport protein. A) The p.H310Y change is predicted to cause major structural alterations to the C-terminus of clavesin-1 and interfere with alpha-tocopherol-binding domain (White arrow). **B-C)** Co-immunoprecipitation studies revealed a decrease in Myc-tagged clavesin-1 bound to the immunoprecipitated Flag-tagged αTTP when both are expressed at equivalent levels in HEK293 cells (N=3, p=0.006, t-test).

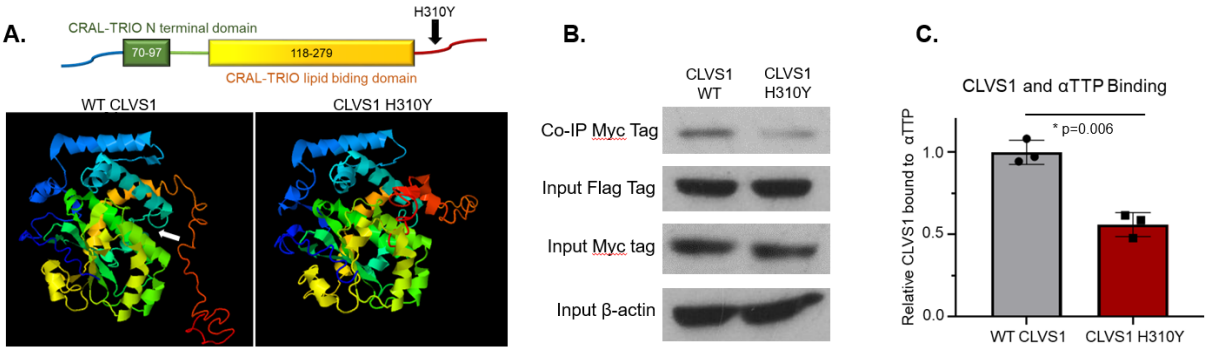

Figure 7: Defective ROS regulation contributes to decreased viability in *CLVS1* KO and H310Y KI podocytes. A-B) Automated live cell imaging and quantification of ROS levels in *CLVS1* KO podocytes as well as controls using a fluorescent reporter of multiple ROS types including hydrogen peroxide, peroxynitrite and hydroxl radicals (A)(N>20 for each group, p<0.0001 for all time points for KO, p<0.05 for all time points, and after 20 mins for KI, two-way ANOVA) as well as a second independent fluorescent reporter that detects superoxide generation (B) (N>20 for each group, p<0.001 for all time points after 10 hours, two-way ANOVA) revealed an increase in ROS and superoxide accumulation in *CLVS1* KO and homozygous KI podocytes that could be rescued with pretreatment with 1µM Dexamethasone. **C-D)** The increased susceptibility to apoptosis in *CLVS1* KO and homozygous KI podocytes (p<0.05 for all time points after 36 hrs) could be rescued by treatment with a superoxide scavenger or an ROS inhibitor (5nM Mito-TEMPO and 500nM Elamipretide) (N>10 for all conditions, two-way ANOVA). The ROS inducer pyocyanin (300uM) and ROS inhibitor N-acetyl-L-cysteine (5mM) were used as positive and negative controls respectively for all experiments. Error bars depict SEM.

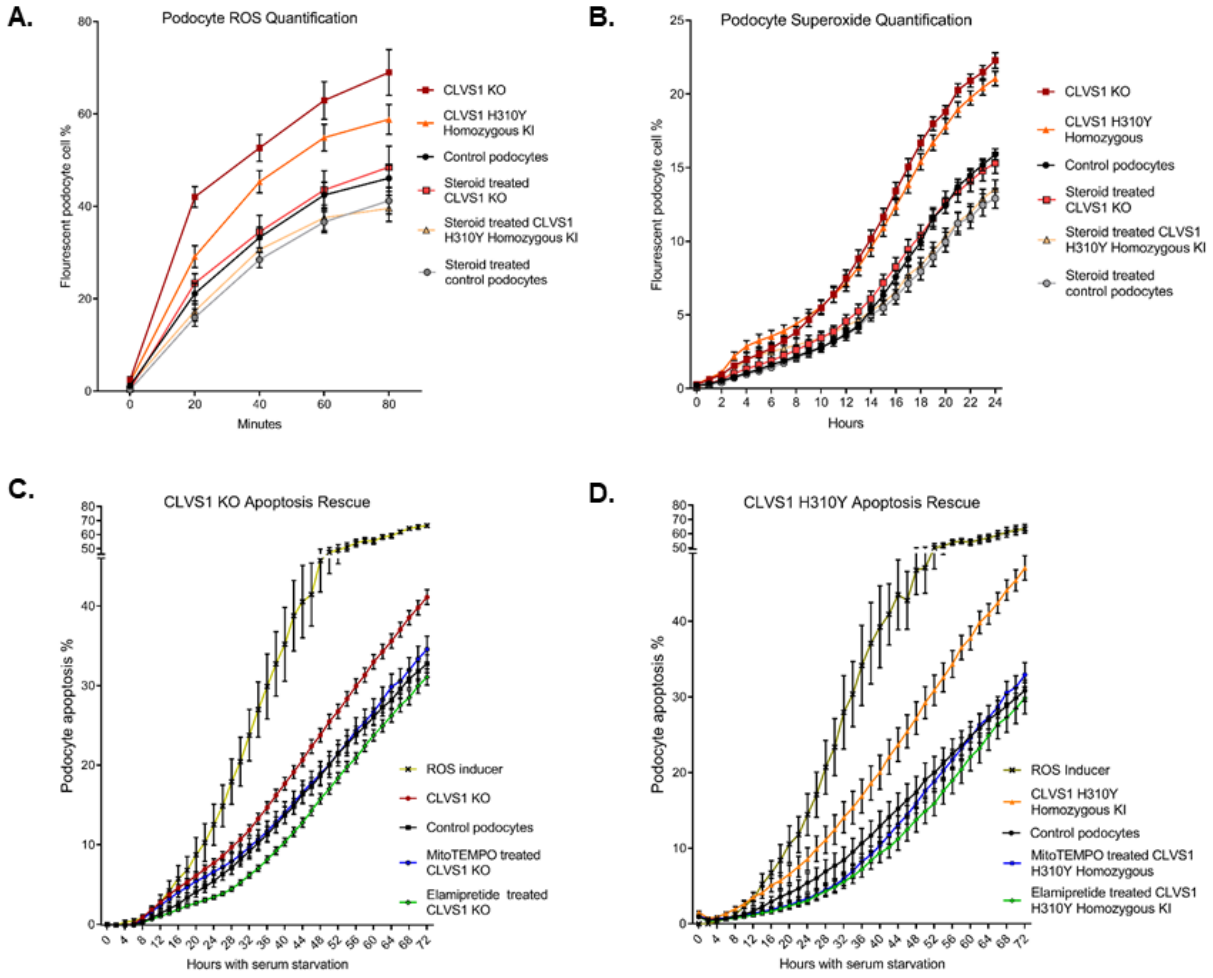

Figure 8: Summary Figure: Based on the data acquired in this study, we posit that *CLVS1* function is required for clathrin-mediated endocytosis in podocytes and disruptions in this process lead to disruption of glomerular filtration barrier resulting in glomerular disease. The p.H310Y variant reduces the CME of key podocyte molecules such as alpha-tocopherol, whose absence drives increased reactive oxygen species and reduces viability. This pathologic condition can be improved by the increased macropinocytosis and antioxidant enzyme activity in podocytes caused by corticosteroid treatment.

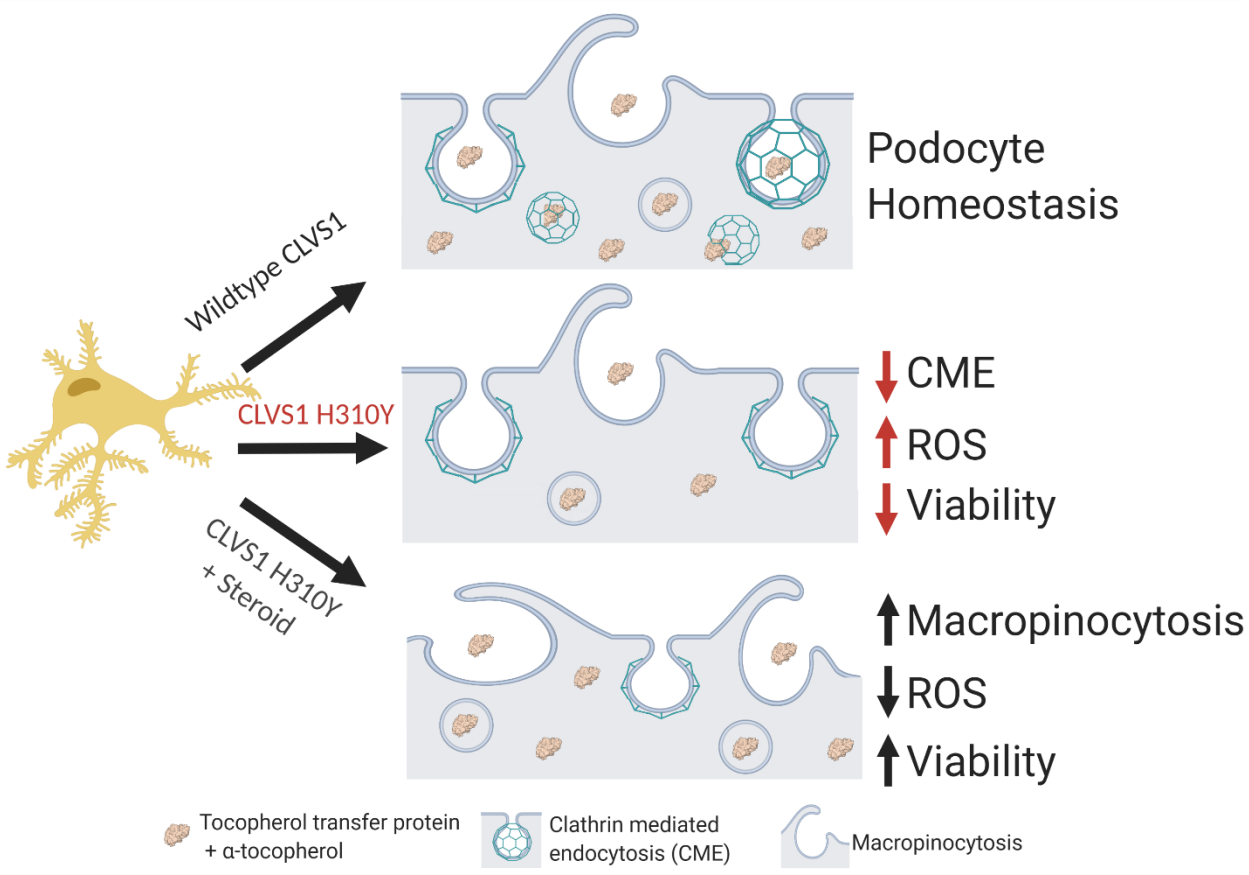

Table 1: Clinical characteristics of family with *CLVS1* mutation

Study no	Sex	Age at onset of disease (years)	Spot urinary protein ratio (g/g)	Kidney Biopsy Y/N (Findings)	SSNS course	Years of Follow up	Response to steroid sparing agents Y/N (Type)
1	Female	8	8.3	Y (mesangial proliferative)	FR/SD	8	Y (Cyclophosphamide)
100	Female	9	3.0	N	FR/SD	2.5	Y (Rituximab)
107	Male	10	UNK	N	FR/SD	UNK	NA

UNK: Unknown, Y: Yes, N: No, FR/SD: Frequent relapsing/steroid dependent,

SSNS: Steroid sensitive nephrotic syndrome, NA: Not applicable

Table 2: Evolutionary conservation of the clavesin-1 H310 residue

Human	K	**H**	T
Rhesus	K	**H**	T
Mouse	K	**H**	T
Dog	K	**H**	T
Elephant	K	**H**	T
Chicken	K	**H**	A
X tropicalis	K	**H**	V